PROCEEDINGS OF SCIENCE

Physical inference from the temporal analysis of PKS 1510-089 during the 2014 – 2015 multi-wavelength flaring events

T. Mbonani* **and B. van Soelen**

Department of Physics, University of the Free State,
205 Nelson Mandela Drive, Bloemfontein, South Africa

E-mail: tekano.motsoari@gmail.com, vansoelenb@ufs.ac.za

Temporal studies have long been employed as tools to probe and investigate the physics in the inner regions of Active Galactic Nucleis (AGNs). PKS 1510-089 is a frequently studied Flat Spectrum Radio Quasar (FSRQ), often showing multi-wavelength quasi-simulataneous observations. We report on the optical and γ-ray temporal analysis focused on major outburst events (flares) in 2014 – 2015. The γ-ray flares are characterized by intra-day variability (IDV), with flux doubling times on the scale of hours. Optical/γ-ray z-transformed Discrete Cross-Correlation Function (ZDCF) analysis revealed significant correlation (>95.45% C.L) between the low and high energy bands, found with near-zero time lags. We determined the minimum Doppler factors from each flare and constrained the γ-ray emission regions to distances close to the inner boundaries of the broad-line region (BLR) away from the central supermassive black hole (SMBH).

High Energy Astrophysics in Southern Africa 2022 - HEASA2022
28 September - 1 October 2022
Brandfort, South Africa

*Speaker

PoS(HEASA2022)053

1. Introduction

PKS 1510-089 (z = 0.361, [1]) is a well known flat-spectrum radio quasar (FSRQ) that continues to be the subject of several extensive multi-wavelength, temporal and spectral variability studies. The radio to very high energy (VHE) γ-ray emission observed during flaring states is believed to originate from quasi-spherical, electron plasmoid regions propagating at relativistic velocities along the jet axis [2]. The multi-wavelength emission is characterized by variability on all accessible time-scales and complex multi-frequency relationships revealed by robust correlation studies [3]. The broadband Spectral Energy Distribution (SEDs) of the target features a low and high energy non-thermal component, with the former ranging from radio to soft X-rays, while the latter extends from hard X-rays to VHE γ-rays [4]. The low energy component is undertood as synchrotron emission from relativistic electrons, while the high energy component can be explained by both leptonic (electron inverse Compton) and hadronic (e.g. proton synchrotron) emission models [5, 6]. Here we present a temporal analysis of four γ-ray flares observed during 2014 – 2015, using the *Fermi*-LAT telescope, correlated against optical photometric observations. These observations were used to place constraints on the emission region. We adopted a flat cosmology with $H_0 = 69.6$ and $\Omega_M = 0.286$ [7].

2. Observations and Data Reduction

2.1 Optical Observations

Optical photometric observations were undertaken using the Watcher Robotic telescope [8] and the 1.0-m class telescopes on the Las Cumbres Observatory (LCO).[1] Additionally, publically available data from the SMARTS survey [9], and Steward Observatory was obtained.[2] Observations were taken with the LCO telescopes using the Sloan filters (g', r', i') while the other observations were taken using Johnston-Cousin filters (U, B, V, R, I). The reduction and photometry of the observations obtained with the Watcher telescope were performed using the pipeline developed by [10]. Standard photometry was performed on the LCO data which had been pre-reduced by **BANZAI**[3] pipeline. The correction from the Sloan to Johnston filters was performed by adopting the second order, colour dependent equations given by [11]. The foreground Galactic extinction was corrected using absorption values from NED (A_λ),[4] based on the re-calibration of the [12] extinction map by [13]. The magnitudes (m_ν) were converted to flux (F_ν) using the reference magnitudes from [14], i.e.,

$$F_\nu = F_0 \times 10^{\left(\frac{m_0 - m_\nu}{2.5}\right)}, \tag{1}$$

where $m_0 = 0$ is the reference magnitude and F_0 (W m^{-2} Hz^{-1}) is the reference flux at zero magnitude adopted from [14].

[1] https://lco.global/observatory/telescopes/1m/.
[2] http://james.as.arizona.edu/~psmith/SPOL
[3] https://lco.global/documentation/data/BANZAIpipeline/
[4] https://ned.ipac.caltech.edu/Documents/Guides/Calculations

2.2 Gamma-ray Observations - *Fermi* LAT

The *Fermi* Large Area Telescope (LAT) is sensitive to γ-rays with energies of 20 MeV to > 300 GeV, and operates in an all sky observing mode [15]. We analysed data within the 0.1–300 GeV energy range between December 2014 – December 2015 (MJD 57000 – 57360). We employed the standard analysis software packages (version V11r5p3) and instrument response function (P8R3_SOURCE_V3_v1) to analyze Pass 8 SOURCE class events within a 15° radius region of interest (ROI) centred at the position of PKS 1510-089. We selected events with a zenith angle < 90° to filter out contamination from the Earth's limb γ-rays. We built an unbinned maximum likelihood model for a region with an additional 10° radius around the ROI, which included emission from spatial point sources from the 4FGL catalogue, the Galactic diffuse emission (gll_iem_v07.fits), the extragalactic diffuse and isotropic residual instrument background emission (iso_P8R3_V3_v1.txt). In the model fits, only PKS 1510-089 (power-law), bright sources (TS > 25), the Galactic and extragalactic diffuse backgrounds had their spectral parameters left free, while other sources were held at their 4FGL catalog values. To investigate source variability we produced light-curves in time bins of 6, 12 and 24 hours, using a power-law spectral function in each time bin with both the photon index and integral flux normalization parameters left free in the model fits. For data points with TS < 9, we estimated upper limits. For the estimation of maximum photon energy from the target, we employed the ULTRACLEAN class template to extract events with energy > 5 GeV, detected with zenith angle θ > 105°, within a ROI with a radius of 0°.5.

3. Results

3.1 Multi-wavelength light-curves

The multi-wavelength light-curves in Figure 1 show the variability of PKS 1510-089 at γ-ray, X-ray (0.3 - 10 keV) and optical frequencies from December 2014 to December 2015. The daily binned γ-ray light-curves (photon cm^{-2} s^{-1}) were scanned using the Fractional root-mean-square (rms) analysis [16], and four major flaring events were identified ($F_{\rm VAR} \geq 0.5$). The flaring events were identified as F1 (MJD 57105 - 57145), F2 (MJD 57152 - 57166), F3 (MJD 57205 - 57235) and F4 (MJD 57240 - 57254). The X-ray flux is taken from [17], obtained with the *Swift* X-ray Telescope (XRT). The optical emission showed the highest variability during the first three flare events, but we caution that the cadence of the observations was lower during the fourth flare. The maximum optical flux was observed during F3 ($F_{\rm R}$ = 1.18×10^{-25} erg cm^{-2} s^{-1} Hz^{-1} at MJD 57222.78), which was the least bright of the flares in γ-rays.

3.2 Gamma-ray temporal profiling & photon energies

In order to study the γ-ray temporal evolution of F1 – F4, we fit the 6 hour binned γ-ray light-curves with double exponential functions [18] and extracted flux doubling times, i.e., times in which the flux changes by a factor of two. The fastest flux doubling times from F1 (11.14 hours), F2 (3.60 hours), F3 (3.15 hours) and F4 (5.43 hours) place the events within the intra-day variability (IDV) category. A γ-ray photon of 36.30 GeV (> 95.45% C.L) energy was detected during the brightest γ-ray flare in F4 (MJD 57246), see Figure 3(b). Other high energy γ-ray photons detected were 12.94 GeV (MJD 57115), 16.57 GeV (MJD 57157) and 14.82 GeV (MJD 57224) during F1,

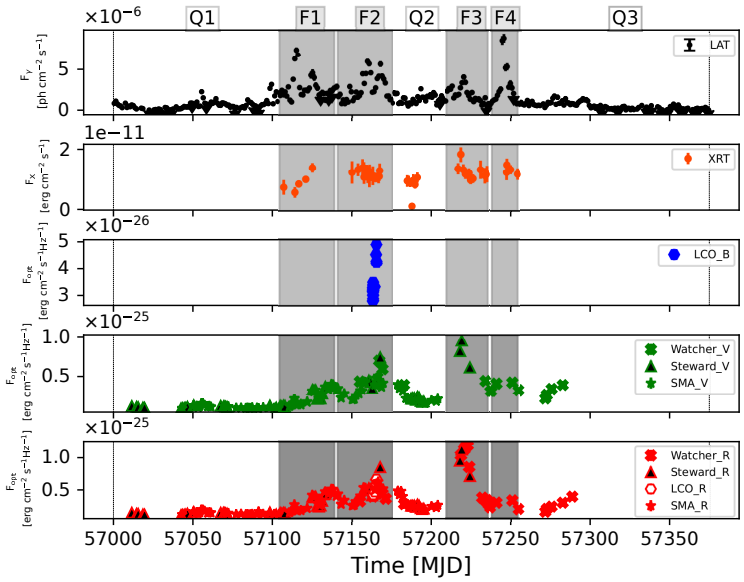

Figure 1: The multi-wavelength light-curves of PKS 1510-089 during 2015. From **top** to **bottom** the figure shows the daily binned γ-ray integral flux [photon cm^{-2} s^{-1}], the X-ray flux [erg cm^{-2} s^{-1}] and the optical flux [erg cm^{-2} s^{-1} Hz^{-1}] in the B, V, R filters, respectively. The identified flaring events are shaded grey.

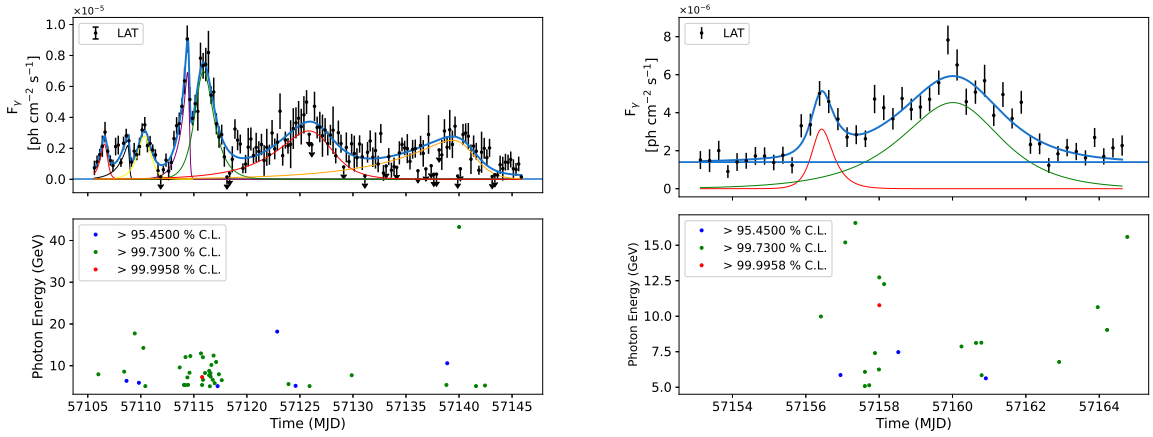

(a) F1 **(b)** F2

Figure 2: The temporal profiling of the γ-ray flares F1 **(a)** and F2 **(b)**. The **top panel** on both **(a)** and **(b)** shows the fitted 6 hour binned γ-ray integral flux. **Bottom panel**: The γ-ray photon energies above 5 GeV detected during F1 **(a)** and F2 **(b)** along with probabilities that photon events are from PKS 1510-089.

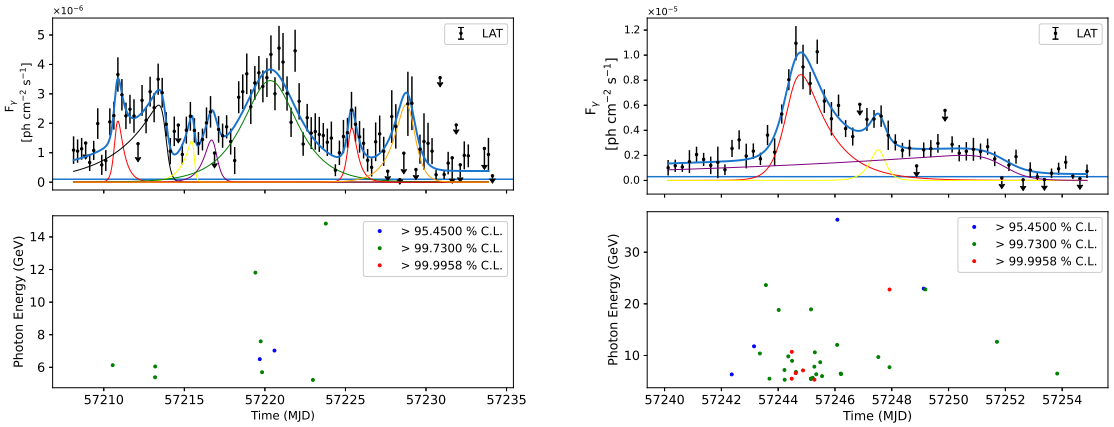

(a) F3 **(b)** F4

Figure 3: The temporal profiling of the γ-ray flares F3 **(a)** and F4 **(b)**. The **top panel** shows the fitted γ-ray integral flux. **Bottom panel**: The γ-ray photon energies above 5 GeV detected during the respective events.

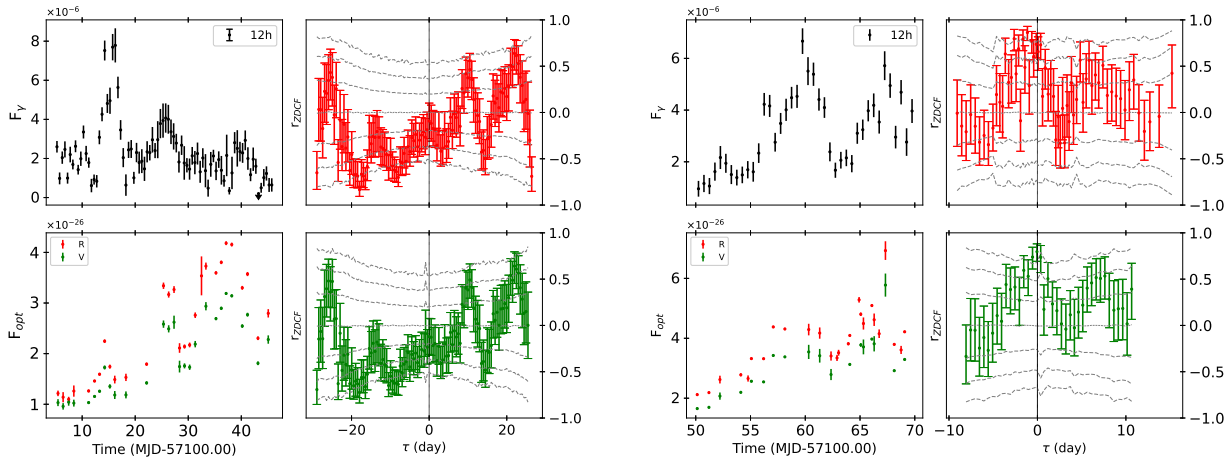

(a) F1 **(b)** F2

Figure 4: The z-transformed discrete cross-correlation functions (ZDCF) of F1 **(a)** and F2 **(b)**. **Top and Bottom Left panels:** The γ-ray and optical R (red), V (green) flux from F1 **(a)** and F2 **(b)**. **Top and Bottom Right panels:** The ZDCF of the γ-ray/optical R (red) and V (green) variation for F1 **(a)** and F2 **(b)**, the grey dashed lines mark the 1σ (68.27%), 2σ (95.45%) and 3σ (99.73%) confidence intervals.

F2 and F3, respectively (Figures 2 and 3(a)). The detection of γ-ray photons implies that they successfully avoided γ-γ absorption. Following this argument, we can evaluate the lower limit on the Doppler factor [19], by assuming the optical depth for the highest energy photon $\tau_{\rm opt} = 1$, i.e.,

$$\delta_{\rm min} = \left[\frac{\sigma_T d_L^2 (1+z)^2 f_{\rm X} \epsilon}{4 t_{\rm var} m_e c^4} \right]^{1/6}, \tag{2}$$

where σ_T is the Thomson scattering cross section, d_L is the luminosity distance of PKS 1510-089, z is the cosmological redshift, $f_{\rm X}$ is the quasi-simultaneous flux in X-rays, $\epsilon = E_\gamma / m_e c^2$ is the γ-ray photon energy and $t_{\rm var}$ is the flux doubling times. Assuming a spherical γ-ray emission region, $t_{\rm var}$ can place limits on the radius of the emission region, i.e., $r \sim c t_{\rm var} \times \delta_{\rm min}/(1+z)$. Similarly, the distance of the emission region relative to the supermassive blackhole (SMBH) can be constrained following,

$$R \geq \frac{2\delta_{\rm min}^2 t_{\rm var} c}{(1+z)}. \tag{3}$$

The Doppler factor $\delta_{\rm min}$ and emission region distance determined for each flare are listed in Table 1.

3.3 Optical & Gamma-ray Cross Correlation

We employed the z-transformed discrete cross correlation functions (ZDCF [20]) to study the correlation between the γ-ray and optical light-curves of events F1 - F2. The ZDCF ($r_{\rm ZDCF}$ = 0.64 ± 0.15) of F1 (Figure 4a) events peaked above the 95.45% C.L, with the γ-ray lagging the optical R variability by τ = 22.00 ± 0.10 days. However, this 22 day delay is consistent with the time between the maximum γ-ray (MJD 57115.50) and optical R (MJD 57138.30) flux. An inspection of the light-curves shows that there are three rise and fall periods in the γ-ray and optical light-curves, and this must be further investigated. For events of F2 (Figure 4b), the ZDCF ($r_{\rm ZDCF}$ = 0.86 ± 0.09) peaked above 3σ (> 99.73% C.L), with the γ-ray leading the optical flare with a near-zero time-lag (τ = -1.13 ± 0.08 days).

4. Discussion and Conclusion

We analyzed the optical and γ-ray light-curves of PKS 1510-089 during active periods between 2014 – 2015. The variability of the source was characterized by four major flaring events labelled F1 – F4. Temporal profiling of the γ-ray flux during flares showed variability on timescales of hours, placing the emission in the IDV category. We found the quasi-simulataneous γ-ray and optical emission to be significantly correlated around the 99.45% confidence level for event F2. A near zero time-lag was seen for the F2 events, which implies that the γ-ray/optical emission were co-spatial in origin. We used $\gamma\gamma$ opacity arguments to determine the Doppler factors and, therefore, the sizes (radii) and distances of the emission regions relative to the SMBH. The fastest flux doubling time (3.15 hrs) from F3 constrained the γ-ray emission region to be 3.66×10^{16} cm ($\geq$ 0.01 pc) away from the SMBH. The derived range of emission region distances from the SMBH, imply that the dominant seed photons needed for EC most likely come from the accretion disk and/or the broad-line region.

	Obs.Dates [2015]	E_γ [GeV]	$t_{\rm var}$ [hours]	$f_{\rm X}$ [erg cm^{-2} s^{-1}]	$\delta_{\rm min}$	r [cm]	R [cm]
F1	24 Mar - 03 May	12.94	11.13	0.85×10^{-11}	6.58	5.81×10^{15}	7.64×10^{16}
F2	10 - 28 May	16.57	3.60	1.38×10^{-11}	8.96	2.56×10^{15}	4.60×10^{16}
F3	07 Jul - 01 Aug	14.82	3.15	1.02×10^{-11}	8.56	2.14×10^{15}	3.66×10^{16}
F4	06 - 20 Aug	36.30	5.43	1.23×10^{-11}	9.36	4.04×10^{15}	7.55×10^{16}

Table 1: Results obtained from the temporal analysis of the major multi-wavelength outbursts from PKS 1510-089 in 2014 – 2015. Parameters: E_γ are γ-ray photon energies, $t_{\rm var}$ are γ-ray flux doubling times, $f_{\rm X}$ are cotemporaneously observed flux in X-ray, $\delta_{\rm min}$ are minimum Doppler factors, R and r are the γ-ray emission region distances relative to the SMBH and sizes (radius) of the emission regions, respectively.

Acknowledgments

We would like to express our gratitude to Dr. R. J. Britto for his contribution and advise on the analysis of the *Fermi*-LAT data and results.

References

[1] D. Thompson, S. Djorgovski and R. De Carvalho, *Spectroscopy of radio sources from the Parkes 2700 MHz survey*, *Publications of the Astronomical Society of the Pacific* **102** (1990) 1235.

[2] V. A. Acciari, S. Ansoldi, L. A. Antonelli, A. Babić, B. Banerjee, U. B. de Almeida et al., *Study of the variable broadband emission of Markarian 501 during the most extreme Swift X-ray activity*, *Astronomy & Astrophysics* **637** (2020) A86.

[3] M. Meyer, J. D. Scargle and R. D. Blandford, *Characterizing the gamma-ray variability of the brightest flat spectrum radio quasars observed with the Fermi LAT*, *The Astrophysical Journal* **877** (2019) 39.

[4] V. Acciari, S. Ansoldi, L. A. Antonelli, A. A. Engels, C. Arcaro, D. Baack et al., *Detection of persistent VHE gamma-ray emission from PKS 1510–089 by the MAGIC telescopes during low states between 2012 and 2017*, *Astronomy & Astrophysics* **619** (2018) A159.

[5] J. Kataoka, G. Madejski, M. Sikora, P. Roming, M. Chester, D. Grupe et al., *Multiwavelength Observations of the powerful gamma-ray quasar PKS 1510–089: Clues on the jet composition*, *The Astrophysical Journal* **672** (2008) 787.

[6] A. Abdo, M. Ackermann, I. Agudo, M. Ajello, A. Allafort, H. Aller et al., *Fermi Large Area Telescope and multi-wavelength observations of the flaring activity of PKS 1510-089 between 2008 September and 2009 June*, *The Astrophysical Journal* **721** (2010) 1425.

[7] P. A. Ade, N. Aghanim, C. Armitage-Caplan, M. Arnaud, M. Ashdown, F. Atrio-Barandela et al., *Planck 2013 results. XV. CMB power spectra and likelihood*, *Astronomy & Astrophysics* **571** (2014) A15.

[8] J. French, L. Hanlon, B. McBreen, S. McBreen, L. Moran, N. Smith et al., *Watcher: A Telescope for Rapid Gamma-Ray Burst Follow-Up Observations*, in *AIP Conference Proceedings*, vol. 727, pp. 741–744, American Institute of Physics, 2004.

[9] D. L. DePoy, B. Atwood, S. R. Belville, D. F. Brewer, P. L. Byard, A. Gould et al., *A novel double imaging camera (ANDICAM)*, in *Instrument Design and Performance for Optical/Infrared Ground-based Telescopes*, vol. 4841, pp. 827–838, SPIE, 2003.

[10] J. P. Marais, *Searching for new very high energy emitting AGN among the unclassifed and unassociated Fermi-LAT sources*, 2019.

[11] A. Kostov and T. Bonev, *Transformation of Pan-STARRS1 gri to Stetson BVRI magnitudes. Photometry of small bodies observations*, *arXiv preprint arXiv:1706.06147* (2017) .

[12] D. J. Schlegel, D. P. Finkbeiner and M. Davis, *Maps of dust infrared emission for use in estimation of reddening and cosmic microwave background radiation foregrounds*, *The Astrophysical Journal* **500** (1998) 525.

[13] E. F. Schlafly and D. P. Finkbeiner, *Measuring reddening with Sloan Digital Sky Survey stellar spectra and recalibrating SFD*, *The Astrophysical Journal* **737** (2011) 103.

[14] M. Bessell, *UBVRI photometry II: the Cousins VRI system, its temperature and absolute flux calibration, and relevance for two-dimensional photometry.*, *Publications of the Astronomical Society of the Pacific* **91** (1979) 589.

[15] W. Atwood, A. A. Abdo, M. Ackermann, W. Althouse, B. Anderson, M. Axelsson et al., *The large area telescope on the Fermi gamma-ray space telescope mission*, *The Astrophysical Journal* **697** (2009) 1071.

[16] S. Vaughan, R. Edelson, R. Warwick and P. Uttley, *On characterizing the variability properties of X-ray light curves from active galaxies*, *Monthly Notices of the Royal Astronomical Society* **345** (2003) 1271.

[17] R. Prince, N. Gupta and K. Nalewajko, *Two-zone Emission Modeling of PKS 1510-089 during the High State of 2015*, *The Astrophysical Journal* **883** (2019) 137.

[18] A. Abdo, M. Ackermann, M. Ajello, E. Antolini, L. Baldini, J. Ballet et al., *Gamma-ray light curves and variability of bright Fermi-detected blazars*, *The Astrophysical Journal* **722** (2010) 520.

[19] V. S. Paliya, *Fermi-large area telescope observations of the exceptional gamma-ray flare from 3c 279 in 2015 june*, *The Astrophysical Journal Letters* **808** (2015) L48.

[20] T. Alexander, *Is AGN Variability Correlated with other AGN Properties?—ZDCF Analysis of Small Samples of Sparse Light Curves*, in *Astronomical Time Series*, pp. 163–166, Springer, (1997).